JCTC Journal of Chemical Theory and Computation

ARTICLE

pubs.acs.org/JCTC

Boxed Molecular Dynamics: Decorrelation Time Scales and the Kinetic Master Equation

David R. Glowacki,*[,†] Emanuele Paci,[‡] and Dmitrii V. Shalashilin[§]

[†]Centre for Computational Chemistry, University of Bristol, Bristol BS8 1TS, United Kingdom

[‡]Institute of Molecular and Cellular Biology, University of Leeds, Leeds LS2 9JT, United Kingdom

[§]School of Chemistry, University of Leeds, Leeds LS2 9JT, United Kingdom

ABSTRACT: A number of methods proposed in the past few years have been aimed at accelerating the sampling of rare events in molecular dynamics simulations. We recently introduced a method called Boxed Molecular Dynamics (BXD) for accelerating the calculation of thermodynamics and kinetics (*J. Phys. Chem. B* **2009**, *113*, 16603−16611). BXD relies upon confining the system in a series of adjacent "boxes" by inverting the projection of the system velocities along the reaction coordinate. The potential of mean force along the reaction coordinate is obtained from the mean first passage times (MFPTs) for exchange between neighboring boxes, simultaneously providing both kinetics and thermodynamics. In this paper, we investigate BXD in the context of its natural relation to a kinetic master equation and show that the BXD first passage times (FPTs) include different time scales—a fast short time decay due to correlated dynamical motion and slower long time decay arising from phase space diffusion. Correcting the FPTs to remove the fast correlated motion yields accurate thermodynamics and master equation kinetics. We also discuss interrelations between BXD and a recently described Markovian milestoning technique and use a simple application to show that, despite each method producing distinct nonstatistical effects on time scales on the order of dynamical decorrelation, both yield similar long-time kinetics.

1. INTRODUCTION

Accurate sampling of rare events remains a significant challenge to molecular dynamics (MD) simulations, and a number of methods have been proposed to address it.[1−27] In a recent publication, we introduced a simple and exact technique for accelerating molecular dynamics (MD) simulations.[28] By slicing a reaction coordinate into "boxes" along some reaction coordinate, short-time dynamics within each box may be analyzed in order to obtain mean first passage times (MFPTs) between neighboring boxes. This method, which we named "boxed" molecular dynamics (BXD), is an extension of the method of classical dynamics accelerated by phase space constraints[29,30] and has its origin in Intramolecular Dynamics Diffusion Theory (IDDT).[31−34] IDDT shows that Newtonian classical molecular dynamics written in the form of the Liouville equation can effectively be replaced by an equation for diffusion along the reaction coordinate.[33,34] In IDDT, the reaction coordinate is divided into boxes, and coefficients for the diffusion equation or the equivalent Langevin equation[31] are determined by short-time MD with initial conditions sampled box by box. Reactions on longer time scales may then be reconstructed from the set of short time simulations by integration. A number of modern techniques, including BXD, are similar in spirit.

Free energies and rate coefficients are among the most important calculable quantities that may be obtained from MD; however, unlike BXD, few methods simultaneously provide both kinetic and thermodynamic information. In this paper, we consider in detail the relationship between the kinetic master equation and the BXD technique. This connection naturally arises because kinetics and thermodynamics are linked in BXD—i.e., thermodynamics are obtained from BXD using box-to-box mean first passage times (MFPTs). Through consideration of the loop formation dynamics of a simple 10-ALA peptide, we show that the distribution of FPTs obtained from BXD includes distinct time scales: fast dynamically correlated motion at short times, with slower diffusional decay at longer times. This separation in FPT time scales is akin to the sorts of dynamical recrossing corrections to transition state theory (TST) rate coefficients which arise from the fluctuation−dissipation theorem.[35−38] In this paper, we show that free energy surfaces obtained with BXD are largely independent of fast correlated motion; however, an accurate calculation of phenomenological kinetics using a kinetic master equation requires that the box-to-box MFPTs are corrected for the fast dynamical motion.

We also consider the relationships between BXD and a recent modification of milestoning[39−41] called Markovian milestoning (MM).[7,8] The distribution of FPTs used to solve the kinetic master equation in Markovian milestoning is distinct from that obtained using BXD, and we show that the difference primarily arises in how each treats the fast correlated motion. Whereas the BXD FPTs include very fast recrossing events, the Markovian milestoning FPTs have an initial short time lag. When the BXD FPTs are corrected for recrossing, they give kinetic master equation solutions in close agreement with those obtained from Markovian milestoning, in addition to providing accurate thermodynamics.

Received: January 5, 2011
Published: April 19, 2011

Scheme 1. Illustration of the AXD Approach (Boxed Molecular Dynamics with Two Boxes) for Calculating Accelerated Reaction Rates[a]

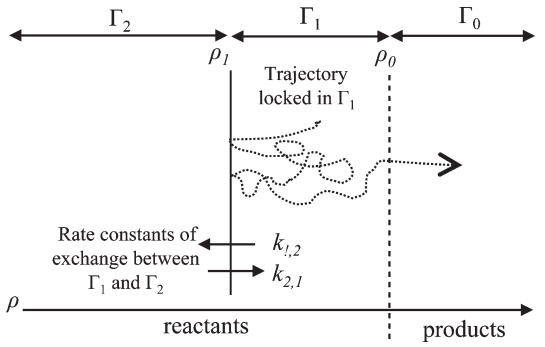

[a] The trajectory simulation locked in Γ_1 provides the accelerated rate coefficient. The correction factor is expressed through phase volumes Γ_1 and Γ_2 (or rate constants k_{12} and k_{21}) as described in the text.

2. BRIEF OVERVIEW OF BOXED DYNAMICS FORMALISM

The technique we introduced previously was composed of two parts (AXD and BXD), which we named differently according to the circumstances of their usage—AXD is an abbreviation of "accelerated dynamics" and is generally intended for accelerating the calculation of rate coefficients in MD, while BXD is intended for accelerating potential of mean force calculations. However, both techniques amount to the same procedure, despite their different intents. The only significant difference is that AXD has two boxes, while BXD has an arbitrary number of boxes. Thus, it is appropriate to refer to both methods as "boxed molecular dynamics". To keep this paper reasonably self-contained, a brief summary of AXD and BXD is included below.

Boxed molecular dynamics relies on the assumption that the classical mechanics of anharmonic systems on time scales above the dynamical decorrelation time, τ_{corr}, are essentially ergodic. In such systems, equilibrium is quickly established between neighboring regions of the system phase space. So long as this is the case, dynamics can be accurately approximated using Markov models (obtained via Monte Carlo methods or short MD trajectories) for describing the exchange between different regions of the phase space.[35−38] Scheme 1 illustrates the main ideas of AXD.

According to classical TST, the phase space of the system is separated into reactant and product regions by a dividing surface at ρ_0 along some reaction coordinate, and the reaction rate coefficient is then calculated as a flux through the dividing surface. AXD accelerates passage through ρ_0 by splitting the reactant phase space into two boxes: Γ_1, which spans ρ_0 to ρ_1, and Γ_2, which is bounded by ρ_1. By locking the dynamics within Γ_1, the trajectory crosses the transition state more often, yielding an accelerated rate coefficient, k^{AXD}. The actual rate coefficient, $k(T)$, of going from the reactant region, $\Gamma_1 + \Gamma_2$, to the product region, Γ_0, may then be recovered as

$$k(T) = k^{AXD} \times P^{CORR} \tag{1}$$

where the P^{CORR} correction factor is the probability of finding the system in Γ_1. Trajectories are confined within Γ_1 by utilizing a velocity inversion algorithm which conserves the total energy, linear momentum, and angular momentum. At each integration time step t, we calculate the trajectory's position along the reaction coordinate. If it moves outside ρ_1 at time step $t + dt$, then we return to the previous step t and invert the projections of the velocities along the reaction coordinate.

Scheme 2. Illustration of the BXD Procedure for a System Partitioned into m "Boxes"[a]

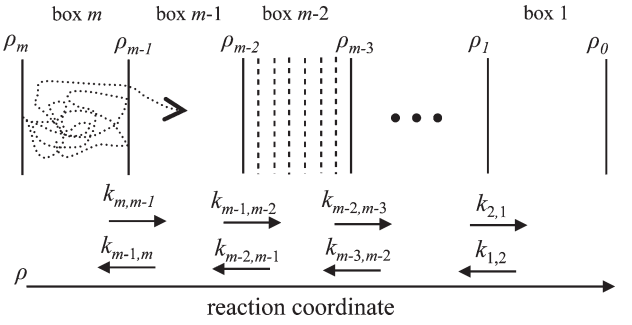

[a] In this simple picture, the trajectory penetrates from box m into box $m - 1$ after two inversions at the ρ_{m-1} boundary.

Provided the assumption of equilibrium between boxes Γ_1 and Γ_2 is valid, P^{CORR} is calculated simply as the fraction of the phase volume Γ_1 to the total reactant phase volume.

$$P^{CORR} = \frac{\Gamma_1}{\Gamma_1 + \Gamma_2} \tag{2}$$

The phase volume ratio in eq 2 may be estimated from a Monte Carlo random walk or by running a trajectory in $\Gamma_1 + \Gamma_2$. Another way to calculate the correction factor is to recognize that the ratio of the two phase volumes is simply the equilibrium constant k_{21} of exchange between Γ_1 and Γ_2, which can be estimated from classical molecular dynamics as a ratio of the box-to-box rate constants k_{12} and k_{21}:

$$P^{CORR} = \frac{1}{1 + \frac{\Gamma_2}{\Gamma_1}} = \frac{1}{1 + K_{21}} = \frac{1}{1 + \frac{k_{12}}{k_{21}}} \tag{3}$$

The fundamental efficiency gain of AXD derives from the fact that it is less expensive to converge k^{AXD} and P^{CORR} separately than their small product $k(T)$, and the bulk of this paper is concerned with how to accurately calculate k_{12} and k_{21}.

If motion along the reaction coordinate involves rare events, then boxed dynamics (BXD), which is a simple extension of AXD, offers a tractable means for obtaining P^{CORR}. The BXD approach is illustrated in Scheme 2, which shows the reaction coordinate ρ split into m intervals by boundaries at ρ_0, ρ_1, ..., ρ_{m-1}, ρ_m. Velocity inversion is carried out at each of the boundaries. By counting the total time t the trajectory spends in a particular box as well as the number of inversions at a particular boundary, the kinetics for "exchange" between the neighboring boxes may be obtained, as described further below.

If the box boundaries are positioned so that there is no irreversible flux through border ρ_0 or ρ_m (i.e., $k_{1,0} = k_{m,m+1} = 0$), one may obtain thermodynamic information along the entire reaction coordinate of a system like that described in Scheme 2 using the box-to-box forward and reverse rate constants. So long as a temperature may be defined, equilibrium constants between the neighboring boxes n and $n - 1$ may be obtained as

follows:

$$K_{n-1,n} = \frac{k_{n-1,n}}{k_{n,n-1}} = \exp\left(\frac{-\Delta G_{n-1,n}}{kT}\right) \quad (4)$$

The free energy difference between each neighboring box, $\Delta G_{n-1,n}$, may then be found by rearranging eq 4. With respect to an arbitrary zero, each box averaged free energy, ΔG_n, may then be determined together with p_n, the equilibrium probability of residing in box n:

$$p_n = \frac{1}{\sum_n \exp(-\Delta G_n/kT)} \exp(-\Delta G_n/kT) \quad (5)$$

The time that the trajectory spends in each box is determined by how long it takes for the rate coefficients in each box to converge. As described in our previous article,[28] the statistics obtained within each box may be placed into smaller histogram bins (represented by the dashed lines in Scheme 2) and then exactly renormalized to provide the probability distribution along the entire reaction coordinate, $p(\rho)$, to a higher resolution.

3. DYNAMICAL DECORRELATION IN AXD

Accurate calculation of the rate constants of "exchange" between the boxes is the key to the AXD and BXD techniques. In this section, we consider in detail how dynamical decorrelation time scales affect the two-box AXD procedure. AXD is based upon eq 1, whose origin may be understood through consideration of the classical canonical TST expression for calculating the reactive flux from the reactant phase space, R, across a dividing surface in phase space. Dividing surfaces in coordinate space are more common than coordinates in phase space because of their relative simplicity; however, we note that the TST hypersurface may be defined by both coordinates, $\mathbf{q}$, and momenta, $\mathbf{p}$. For the purposes of this article, we simply and generally write the TST rate coefficient as

$$k^{\mathrm{TST}}_{R\rightarrow}(T) = \frac{\langle|v|\delta(\mathbf{q},\mathbf{p})\,\Theta(\mathbf{q},\mathbf{p})\rangle}{\Gamma_R} \quad (6)$$

where $|v|$ is the magnitude of the velocity vector normal to the transition state dividing surface in phase space, $\Theta(\mathbf{q},\mathbf{p})$ is an indicator function which is unity when the system is in state R and zero otherwise, and $\delta(\mathbf{q},\mathbf{p})$ is a Dirac δ function which is unity at the dividing surface. The numerator in eq 6 uses angled brackets $\langle ... \rangle$ to indicate that it is the Boltzmann weighted average of velocities perpendicular to the TS dividing surface which are leaving R. The integral in the denominator is the reactant phase space volume Γ_R. The logic of Scheme 1 and the corresponding basis for eq 1 derives from the fact that the reactant phase space $\Gamma_R = \Gamma_1 + \Gamma_2$, which allows eq 6 to be written as

$$\begin{aligned} k^{\mathrm{TST}}_{R\rightarrow}(T) &= \frac{\langle|v|\delta(\mathbf{q},\mathbf{p})\,\Theta(\mathbf{q},\mathbf{p})\rangle}{\Gamma_1+\Gamma_2} \\ &= \frac{\langle|v|\delta(\mathbf{q},\mathbf{p})\,\Theta(\mathbf{q},\mathbf{p})\rangle}{\Gamma_1} \times \frac{\Gamma_1}{\Gamma_1+\Gamma_2} \\ &= k^{\mathrm{AXD}} \times P^{\mathrm{CORR}} \end{aligned} \quad (7)$$

Neither eq 6 nor eq 7 include corrections for motion on time scales smaller than that of τ_{corr},[35−38] which enters in the form of a scaling factor, κ, reducing the magnitude of the flux through the TST dividing surface:

$$\begin{aligned} \kappa k^{\mathrm{TST}}_{R\rightarrow}(T) &= \kappa\frac{\langle|v|\delta(\mathbf{q},\mathbf{p})\,\Theta(\mathbf{q},\mathbf{p})\rangle}{\Gamma_1} \times \frac{\Gamma_1}{\Gamma_1+\Gamma_2} \\ &= \kappa k^{\mathrm{AXD}} \times P^{\mathrm{CORR}} \end{aligned} \quad (8)$$

Equation 8 shows that κ is an effective scaling factor to the accelerated rate coefficient, k^{AXD}, in the same way that it is for k^{TST}; this is because the rapid dynamical motion for which κ accounts is localized in the phase space neighborhood of the dividing surface. The correction factor P^{CORR}, being an equilibrium property of the system, is applied in exactly the same fashion whether or not κ is included, and this holds so long as Γ_1 is larger than the dynamical decorrelation length scale near the dividing surface ρ_0 (see Scheme 1).

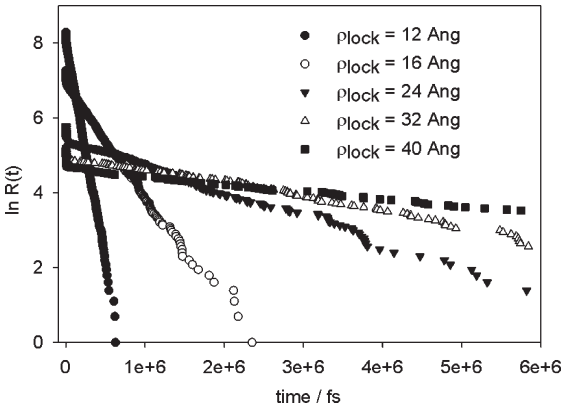

Figure 1. AXD decay traces at varying values of ρ_1 where ρ_1 is equivalent to ρ_{lock}. Each trace shows a fast decay at short times deriving from recrossing and a slow decay at longer times.

Consideration of fast dynamical motion on passage through the dividing surface ρ_0 is critical to obtaining an accurate estimate of the unbiased rate coefficient. Below, we illustrate this point for the loop formation dynamics of a 10-alanine peptide where the reaction coordinate, ρ, is the distance between the main-chain nitrogen on the N-terminal residue and the carboxyl carbon of the C terminal residue—i.e., the peptide extension.[42,43] We ran dynamics using a CHARMM19 force field and a simple implicit solvation model.[44] With this force field, 10-alanine turns out to have a strong helical propensity. The MD was run for 1 μs using Langevin dynamics with a friction coefficient of 1 ps^{-1} and a time step of 1 fs. The transition state ρ_0 between reactants (the extended peptide) and the product (the peptide which formed a loop) was chosen at a separation of 4.7 Å, near the free energy barrier to contact formation, which was determined in our previous article.[28]

In what follows, we consider the survival probability (or decay trace), $R(t)$, obtained from the lifetime distribution $N(t)$ for passage across a particular boundary within a particular box. In general, $R(t) = \int_0^{t_{\max}} N(t')\,dt' - \int_0^t N(t')\,dt'$ where $t_{\max}$ is the maximum lifetime in the distribution. Figure 1 nicely illustrates the principles discussed above in eqs 6−8. It shows $R(t)$ obtained from FPTs through ρ_0, where ρ_0 is the loop formation TS dividing surface separating Γ_1 from Γ_0 in Scheme 1. $R(t)$ traces were obtained by running a single long trajectory constrained to remain within Γ_1 and Γ_0 and are shown at different values of ρ_1. Each of the traces in Figure 1 clearly shows two different decay time scales—typical of those often observed in studies of

Table 1. AXD Results of the Loop Formation Rate Obtained with Different Values of ρ_1[a]

ρ_1/Å	k^{AXD}/s^{-1}	P^{CORR}	$(k^{AXD}P^{CORR}) \pm \sigma/s^{-1}$
10	2.87×10^{10}	0.021	$(1.29 \pm 0.65) \times 10^9$
12	8.77×10^9	0.045	$(1.05 \pm 0.74) \times 10^9$
16	1.50×10^9	0.099	$(1.05 \pm 0.50) \times 10^9$
20	7.93×10^8	0.649	$(7.90 \pm 3.60) \times 10^8$
24	1.12×10^9	0.985	$(1.12 \pm 0.36) \times 10^9$

[a] The corrected rate coefficients, $k^{AXD}P^{CORR}$, are given in the final column and plotted in Figure 2.

nonstatistical effects in trajectory simulations of chemical reactions.[29,45] The very fast decay of $R(t)$ at short times in Figure 1 arises from fast recrossing through the ρ_0 surface within the dynamical decorrelation time scale, τ_{corr}, and does not vary significantly with different locations of ρ_1 (in Figure 1, ρ_1 is equivalent to ρ_{lock} to maintain consistency with notation used in our previous paper).[28] The slower decay at long times arises from trajectories that have lost dynamical memory within Γ_1 before subsequent ρ_0 crossings. The long time $R(t)$ decay profiles in Figure 1 are inversely proportional to Γ_1. Only by removing the very fast decay events in Figure 1 is it possible to obtain MFPTs and rate coefficients that are statistically identical when scaled by the appropriate values of P^{CORR}, and this is the procedure that we adopted for the results reported in our previous paper.[46] Table 1 and Figure 2 give the corrected rate coefficients, $k^{AXD}P^{CORR}$, where k^{AXD} has been determined from the long time $R(t)$ decay.

4. DYNAMICAL DECORRELATION IN BXD

Having described how to account for nonergodic dynamical motion in two-box AXD simulations, we now turn to multiple-box BXD simulations. At the outset, we note that the methodology described above is similarly applicable. A convenient starting point for the discussion in this section begins by considering BXD's straightforward relation to the kinetic master equation. Assuming for the moment that BXD has provided us with a set of average box-to-box rate coefficients, then the global time dependence of any box population may be described using a set of coupled first-order differential equations:

$$\begin{aligned}
\frac{dn_1(t)}{dt} &= -(k_{21} + k_{10})n_1(t) + k_{21}n_2(t) \\
\frac{dn_2(t)}{dt} &= k_{12}n_1(t) + k_{32}n_2(t) - (k_{21} + k_{23})n_2(t) \\
&\cdots \\
\frac{dn_m(t)}{dt} &= (k_{m-1,m}n_{m-1}(t) - k_{m,m-1}n_m(t)
\end{aligned} \tag{9}$$

Equation 9 is a discretized kinetic master equation (ME),[47−54] where k_{ij} is an average rate coefficient for transfer from box i to its neighboring box j. The equation for n_1 is written assuming that passage across boundary ρ_0 is irreversible.

The whole set of coupled differential equations may be expressed as a matrix eigenvalue problem

$$\frac{d\mathbf{n}(t)}{dt} = \mathbf{M}\mathbf{n}(t) \tag{10}$$

where $\mathbf{n}(t)$ is a vector containing the time dependent populations of each box and $\mathbf{M}$ is the matrix of rate coefficients in eq 9.

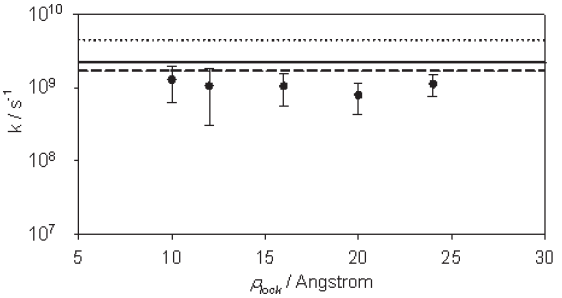

Figure 2. Corrected rate coefficients for contact formation at different values of ρ_{lock}. Also shown are the eigenvalues of smallest magnitude obtained from solving the kinetic master equation using the following methods to obtain transition probabilities: from MFPTs in column 3 of Table 2 (· · · · ·), from corrected MFPTs in column 4 of Table 2 (—), and from milestoning MFPTs in column 3 of Table 3 (----).

Solution of eq 10 provides the time dependence of $\mathbf{n}(t)$ and has the form

$$\mathbf{n}(t) = \mathbf{U}e^{\lambda t}\mathbf{U}^{-1}\mathbf{n}(0) \tag{11}$$

where $\mathbf{n}(0)$ contains the initial conditions for each box, $\mathbf{U}$ is the eigenvector matrix obtained from diagonalization of $\mathbf{M}$, and λ is a vector of the corresponding eigenvalues, where the total number of eigenvalues is equal to m, the number of boxes. An important property of the matrix $\mathbf{M}$ is that the lowest few eigenvalues are often isolated from the other eigenvalues. In such cases, the smallest eigenvalues determine the time scale of kinetic evolution —an example of which is given below.

In boxed MD simulations, practical determination of the rate coefficients for transfer from a particular box to neighboring boxes utilizes the inverse of the mean first passage time (MFPT), $\langle\tau\rangle$. The simplest way to calculate $\langle\tau\rangle$ is by keeping track of (1) how many times a trajectory is inverted at a particular boundary, h, and (2) the lifetime of the trajectory in a particular box. For example, if we run constrained dynamics in box i, which is bounded by ρ_i and ρ_{i-1}, the respective rate coefficients for transfer from box $i \rightarrow i-1$ and box $i \rightarrow i+1$ are

$$\begin{aligned}
k_{i,i-1} &= \langle\tau_{i,i-1}\rangle^{-1} = \frac{h_{i,i+1}}{t_i} \\
k_{i,i+1} &= \langle\tau_{i,i+1}\rangle^{-1} = \frac{h_{i,i-1}}{t_i}
\end{aligned} \tag{12}$$

where t_i is the lifetime of the trajectory in box i and $h_{i,i-1}$ and $h_{i,i+1}$ are the respective numbers of hits (i.e., velocity inversions) at the walls ρ_{i-1} and ρ_{i+1}. When eq 12 is corrected for the effects of fast correlated motion in the same way as AXD, eq 12 may be rewritten as

$$\begin{aligned}
\kappa k_{i,i-1} &= \kappa\langle\tau_{i,i-1}\rangle^{-1} \\
\kappa k_{i,i+1} &= \kappa\langle\tau_{i,i+1}\rangle^{-1}
\end{aligned} \tag{13}$$

When BXD is used in order to obtain free energy surfaces by rearranging eq 4, the box-to-box MFPTs *per se* are never required—only their ratio. Thus, the effects of dynamical decorrelation in the forward and reverse directions cancel if they are approximately equal—i.e., $\kappa \approx \kappa_{i,j} \approx \kappa_{j,i}$, an assumption which is discussed further below.

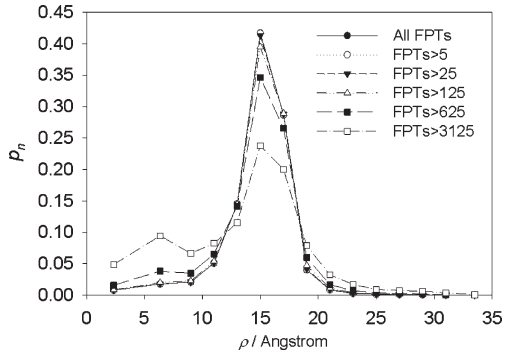

Figure 3. Box averaged probabilities along the reaction coordinate ρ obtained using eq 15 and eq 5. The plot compares box averaged probabilities obtained using values for τ_{corr} of 0, 5, 25, 125, 625, and 3125 fs. The latter two free energy profiles deviate significantly from the others.

The role of κ is to remove fast events on the dynamical decorrelation time scale, τ_{corr}, from the inverse MFPTs, $\langle\tau\rangle^{-1}$, in eq 12. Another way to accomplish this is to replace $\langle\tau\rangle$ with $\langle\tau'\rangle$ using the following equation:

$$\kappa k_{i,i-1} = \langle\tau'_{i,i-1}\rangle^{-1} = \left(\frac{\sum_k \tau_{i,i-1}\theta(\tau^k_{i,i-1} - \tau_{corr})}{\sum_k \theta(\tau^k_{i,i-1} - \tau_{corr})}\right)^{-1}$$

$$\kappa k_{i,i+1} = \langle\tau'_{i,i+1}\rangle^{-1} = \left(\frac{\sum_k \tau_{i,i+1}\theta(\tau^k_{i,i+1} - \tau_{corr})}{\sum_k \theta(\tau^k_{i,i+1} - \tau_{corr})}\right)^{-1} \quad (14)$$

where k is an index that runs over all of the individual first passage times obtained in going from box i toward respective boxes $i-1$ and $i+1$, and $\theta(t)$ is an indicator function which is zero when $t < 0$ and unity otherwise. Equation 14 calculates $\langle\tau'\rangle$ as a MFPT which excludes events shorter than τ_{corr}. In the limit that $\tau_{corr} = 0$, then $\langle\tau\rangle$ in eq 12 is identical to $\langle\tau'\rangle$ in eq 14.

Replacing the values of k in eq 4 with the values of $\langle\tau'\rangle$ in eq 14 yields

$$K_{n-1,n} = \frac{\langle\tau'_{n-1,n}\rangle^{-1}}{\langle\tau'_{n,n-1}\rangle^{-1}} = \exp\left(\frac{-\Delta G_{n-1,n}}{kT}\right) \quad (15)$$

enabling one to subsequently calculate box averaged probabilities, p_n, with eq 5. The difference between eq 4 and eq 15 is that the latter includes corrections to the MFPTs which account for motion on the time scale of τ_{corr}. Figure 3 shows the box averaged probability distributions calculated using eq 15 and eq 5 at values for τ_{corr} ranging from 0 to 3125 fs with τ_{corr} arbitrarily chosen as 5^0, 5^1, 5^2, etc. In these simulations, the reaction coordinate was split into 16 boxes, with indices 0−15, using the box boundaries given in Table 2. The box-to-box values for $\langle\tau'\rangle^{-1}$ (with $\tau_{corr} = 0$ and 125 fs) are given in Table 2. The probability distributions in Figure 3 are statistically indistinguishable for values of τ_{corr} from 0 to 125 fs. Beyond 125 fs, the results start to change significantly. The decorrelation time scale, τ_{corr}, will vary from system to system; however, analysis of the sort shown in Figure 3 helps to place a quantitative upper limit on its value for any particular system and suggests that BXD is a robust method for obtaining PMFs in molecular systems.

Table 2. Inverse MFPTs Obtained Using eq 14 for the 15 Box System Described in the Text[a]

box index			
i	j	$\langle\tau'_{ij}\rangle^{-1}$/fs^{-1}	$\langle\tau'_{ij}\rangle^{-1}$/ fs^{-1}
1 (4.7−8 Å)	0 (0−4.7 Å)	4.33×10^{-7}	2.17×10^{-7}
1 (4.7−8 Å)	2 (8−10 Å)	9.73×10^{-7}	4.94×10^{-7}
2 (8−10 Å)	1 (4.7−8 Å)	8.36×10^{-7}	4.37×10^{-7}
2 (8−10 Å)	3 (10−12 Å)	1.86×10^{-6}	9.33×10^{-7}
3 (10−12 Å)	2 (8−10 Å)	7.53×10^{-7}	3.91×10^{-7}
3 (10−12 Å)	4 (12−14 Å)	1.88×10^{-6}	9.20×10^{-7}
4 (12−14 Å)	3 (10−12 Å)	6.59×10^{-7}	3.44×10^{-7}
4 (12−14 Å)	5 (14−16 Å)	1.77×10^{-6}	8.55×10^{-7}
5 (14−16 Å)	4 (12−14 Å)	6.14×10^{-7}	3.12×10^{-7}
5 (14−16 Å)	6 (16−18 Å)	1.63×10^{-6}	8.43×10^{-7}
6 (16−18 Å)	5 (14−16 Å)	2.38×10^{-6}	1.15×10^{-6}
6 (16−18 Å)	7 (18−20 Å)	3.87×10^{-7}	1.87×10^{-7}
7 (18−20 Å)	6 (16−18 Å)	2.76×10^{-6}	1.14×10^{-6}
7 (18−20 Å)	8 (20−22 Å)	4.39×10^{-7}	2.04×10^{-7}
8 (20−22 Å)	7 (18−20 Å)	2.13×10^{-6}	8.92×10^{-7}
8 (20−22 Å)	9 (22−24 Å)	6.27×10^{-7}	2.93×10^{-7}
9 (22−24 Å)	8 (20−22 Å)	2.00×10^{-6}	8.54×10^{-7}
9 (22−24 Å)	10 (24−26 Å)	6.91×10^{-7}	3.30×10^{-7}
10 (24−26 Å)	9 (22−24 Å)	1.46×10^{-6}	6.58×10^{-7}
10 (24−26 Å)	11 (26−28 Å)	1.05×10^{-6}	4.93×10^{-7}
11 (26−28 Å)	10 (24−26 Å)	1.34×10^{-6}	6.19×10^{-7}
11 (26−28 Å)	12 (28−30 Å)	9.92×10^{-7}	4.52×10^{-7}
12 (28−30 Å)	11 (26−28 Å)	1.54×10^{-6}	6.77×10^{-7}
12 (28−30 Å)	13 (30−32 Å)	7.40×10^{-7}	3.24×10^{-7}
13 (30−32 Å)	12 (28−30 Å)	2.72×10^{-6}	1.08×10^{-6}
13 (30−32 Å)	14 (32−35 Å)	1.87×10^{-7}	8.70×10^{-8}
14 (32−35 Å)	13 (30−32 Å)	5.94×10^{-6}	2.05×10^{-6}
smallest eigenvalue		4.50×10^{-9}	2.20×10^{-9}

[a] The inverse MFPTs in column 3 were obtained with $\tau_{corr} = 0$ fs. Those in the fourth column were obtained with $\tau_{corr} = 125$ fs. The eigenvalues of smallest absolute magnitude, obtained from solution of the kinetic master equation with each set of corresponding inverse MFPTs are given in the last row.

Figure 3 is consistent with the fact that local dynamical motion on the order of the τ_{corr} is approximately identical in both the forward and backward directions. A simple rationalization of the agreement between the box averaged probability distributions in Figure 3 begins from writing the MFPT for transfer from box i to j as

$$\langle t_{ij}\rangle = \alpha_{ij}^{corr}\langle t_{ij}^{corr}\rangle + \alpha_{ij}^{diff}\langle t_{ij}^{diff}\rangle \quad (16)$$

where $\langle t_{ij}^{corr}\rangle$ is the average decorrelation time, $\langle t_{ij}^{diff}\rangle$ is the average decay at times longer than τ_{corr}, which corresponds to diffusive box-to-box motion, and $\langle\alpha_{ij}^{corr}\rangle$ and $\langle\alpha_{ij}^{diff}\rangle$ are the respective fractions of these decay times. So long as the box is large enough, then $\langle t_{ij}\rangle$ is dominated by the longer time motion—i.e.,

$$\langle t_{ij}\rangle \approx \alpha_{ij}^{diff}\langle t_{ij}^{diff}\rangle \quad (17)$$

In the ergodic approximation, the same incoming trajectories are balanced by outgoing trajectories on the shared boundary between boxes i and j. In this limit, it is reasonable to assume

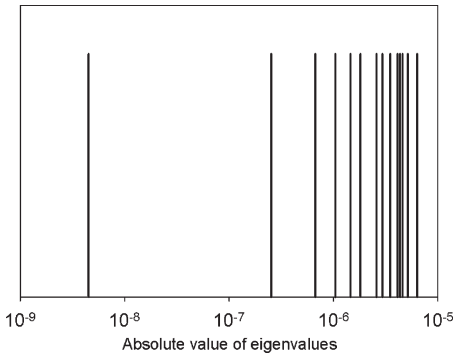

Figure 4. A typical spectrum of the absolute values of the eigenvalues obtained from diagonalization of **M** for the 10-ALA example considered in this work. Loop formation kinetics are dominated by the eigenvalue of smallest absolute magnitude, which is well separated from the others.

that the fraction of diffusive trajectories (those that decorrelate following inversion at the boundary) is approximately the same in both the forward and reverse directions across a particular boundary—i.e., $\alpha_{ij}^{\mathrm{diff}} \approx \alpha_{ji}^{\mathrm{diff}}$ which implies that $\alpha_{ij}^{\mathrm{corr}} \approx \alpha_{ji}^{\mathrm{corr}}$. Hence, the ratio of the rate constants required in eq 4 depends only on the long time decay

$$\frac{k_{ij}}{k_{ji}} \approx \frac{\langle \tau_{ij}^{\mathrm{diff}} \rangle^{-1}}{\langle \tau_{ji}^{\mathrm{diff}} \rangle^{-1}} \tag{18}$$

The same is not, however, true for the kinetics: solutions to the kinetic master equation (eqs 9−11) are rather more sensitive to dynamical corrections than the box averaged probabilities. If **M** is constructed using MFPTs corrected for dynamical decorrelation, then the eigenvalue of smallest absolute magnitude (i.e., the rate coefficient for loop formation kinetics) is in significantly better agreement with the unbiased rate coefficients shown in Table 1 and Figure 2. To demonstrate this fact, we used the data in Table 2 to solve the kinetic master equation. Passage over ρ_0 (the loop formation boundary at 4.7 Å for transfer from box 0⟶1) was treated as an irreversible channel. Other than the boxes at the extrema of the extension reaction coordinate, which have only one set of outgoing transition probabilities, each box in Table 2 has both an ingoing and an outgoing $\langle \tau' \rangle^{-1}$. The final row of Table 2 gives the eigenvalue of smallest magnitude obtained from diagonalization of **M** using MFPTs obtained with eq 14 and τ_{corr} equal to 0 and 125 fs.

The inverse MFPTs in Table 2 result in **M** having one zero eigenvalue, with all of the others negative. Inspection of the eigenvalue spectrum of **M** in Figure 4 shows a single eigenvalue that is well separated from all the others by more than an order of magnitude. Given the separation in eigenvalues, it is a good approximation to represent the system loop formation kinetics using a single exponential term containing the unique eigenvalue. The recrossing corrected inverse MFPTs in the fourth column of table two (τ_{corr} = 125 fs.) are roughly half as large as those which are uncorrected (i.e., τ_{corr} = 0 fs), and the effect on the corresponding eigenvalues is approximately the same, with the corrected eigenvalues in better agreement with results obtained from unbiased simulations (see Figure 1).

5. SHORT TIME BEHAVIOR IN BXD AND MILESTONING

Another method that shares similarities with the BXD technique is milestoning,[7,8,14] which uses short time dynamics to recover local kinetic information about the motion along the reaction coordinate in order to solve a kinetic state-to-state master equation. In particular, a recent variant of milestoning called Markovian milestoning[7] has been proposed wherein the dynamics initiated between a set of milestones are locked so that they cannot escape; however, the kinetic master equation is different for each technique: BXD describes box-to-box transfer, whereas milestoning describes boundary-to-boundary transfer. BXD's formulation arises from a sort of transition state theory (TST) intuition typical in chemistry where we tend to think of chemical reactions in terms of a reactant phase space bounded by a TS dividing surface. This allows us to easily think in terms of a "box averaged free energy".

A milestone, on the other hand, is an infinitesimal slice of phase space along some reaction coordinate. Markovian milestoning utilizes different sets of transition probabilities, depending

Scheme 3. Illustration of the Time Propagation, *t*, of a Constrained Trajectory, along with a Table That Illustrates the Manner in Which FPTs Are Calculated for Both BXD and Milestoning

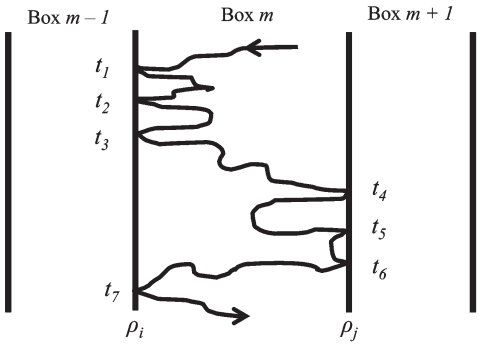

BXD FPTs		Milestoning FPTs	
$m \rightarrow m+1$	$m \rightarrow m-1$	$m \rightarrow m+1$	$m \rightarrow m-1$
$t_5 - t_4$	$t_2 - t_1$	$t_4 - t_1$	$t_7 - t_4$
$t_6 - t_5$	$t_3 - t_2$		
	$t_7 - t_3$		

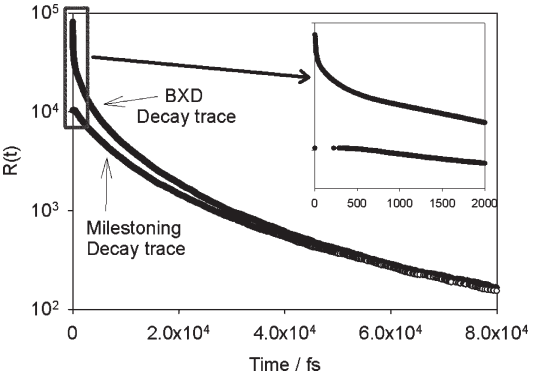

Figure 5. Typical comparison of the decay traces, $R(t)$, generated from the definition of BXD FPTs and milestoning FPTs for the 10-ALA model system. The BXD decay is for transfer from box 2 (spanning ρ = 4.7 Å to ρ = 8.0 Å) to box 1 (spanning ρ = 4.7 Å to ρ = 0.0 Å), whereas the milestoning decay corresponds to transit from milestone 2 (ρ = 8.0 Å) to milestone 1 (ρ = 4.7 Å). The inset shows the different short time behavior for each decay trace.

Table 3. Rate Coefficients Used to Solve the Kinetic Master Equation Obtained by Obtaining MFPTs from the Milestoning Decay Traces[a]

milestone position		
i	j	k_{ij}/fs^{-1}
1 (8 Å)	0 (4.7 Å)	9.00×10^{-8}
0 (4.7 Å)	1 (8 Å)	1.44×10^{-7}
2 (10 Å)	1 (8 Å)	3.31×10^{-7}
1 (8 Å)	2 (10 Å)	6.07×10^{-7}
3 (12 Å)	2 (10 Å)	3.02×10^{-7}
2 (10 Å)	3 (12 Å)	6.08×10^{-7}
4 (14 Å)	3 (12 Å)	2.54×10^{-7}
3 (12 Å)	4 (14 Å)	5.96×10^{-7}
5 (16 Å)	4 (14 Å)	1.87×10^{-7}
4 (14 Å)	5 (16 Å)	4.62×10^{-7}
6 (18 Å)	5 (16 Å)	7.10×10^{-7}
5 (16 Å)	6 (18 Å)	1.42×10^{-7}
7 (20 Å)	6 (18 Å)	6.62×10^{-7}
6 (18 Å)	7 (20 Å)	1.47×10^{-7}
8 (22 Å)	7 (20 Å)	5.75×10^{-7}
7 (20 Å)	8 (22 Å)	2.17×10^{-7}
9 (24 Å)	8 (22 Å)	6.16×10^{-7}
8 (22 Å)	9 (24 Å)	2.47×10^{-7}
10 (26 Å)	9 (24 Å)	5.54×10^{-7}
9 (24 Å)	10 (26 Å)	4.23×10^{-7}
11 (28 Å)	10 (26 Å)	5.41×10^{-7}
10 (26 Å)	11 (28 Å)	3.80×10^{-7}
12 (30 Å)	11 (28 Å)	5.44×10^{-7}
11 (28 Å)	12 (30 Å)	2.74×10^{-7}
13 (32 Å)	12 (30 Å)	9.48×10^{-7}
12 (30 Å)	13 (32 Å)	8.00×10^{-8}
smallest eigenvalue		1.70×10^{-9}

[a] Eigenvalues were obtained by diagonalization of a 14 × 14 matrix.

on what is being calculated: (1) box-to-box MFPTs of the sort written in eq 12 are used to construct free energies, and (2) milestone-to-milestone FPTs are used to construct the kinetic master equation. These different approaches result in different counting algorithms for computing FPTs in the kinetic master equation, which are illustrated in Scheme 3. In the BXD approach, the passage times from box to box (i.e., $m \rightarrow m + 1$, and $m \rightarrow m - 1$ in Scheme 3) are defined as the times between subsequent hits at a particular box boundary; in Markovian milestoning, they are defined as the time it takes to go from milestone to milestone (i.e., $\rho_i \rightarrow \rho_j$, and $\rho_j \rightarrow \rho_i$ in Scheme 3).

Figure 5 shows a typical comparison of the decay traces generated from the definition of BXD FPTs and milestoning FPTs for the 10-ALA model system. The BXD decay shown in Figure 5 corresponds to that from box 2 (spanning $\rho = 4.7$ Å to $\rho = 8.0$ Å) to box 1 (spanning $\rho = 4.7$ Å to $\rho = 0.0$ Å), whereas the milestoning decay corresponds to transit from milestone 2 ($\rho = 8.0$ Å) to milestone 1 ($\rho = 4.7$ Å). The difference in the short time decays between milestoning and BXD arises from the fact that the BXD decays include very fast short time events on the time scale of dynamical decorrelation, which are schematically illustrated in Scheme 3. By contrast, milestone-to-milestone FPTs show a lag in the decay at short times as the trajectory makes a transit from one box edge to another, effectively eliminating the short time dynamical motion. At time scales longer than the short-time milestoning plateau, Figure 5 clearly illustrates that the BXD and milestoning decay traces converge. Table 3 gives the milestone to milestone rate coefficients for the simple 10 ALA model system, as well as the eigenvalue of smallest magnitude obtained from diagonalization of the corresponding rate coefficient matrix.

6. CHARACTERISTIC TIMES

Several characteristic times have emerged in the analysis we have presented in this paper, and their consideration sheds further light on the general applicability of BXD, Markovian milestoning, and other related techniques. The shortest time scale considered in this work is that of dynamical decorrelation, τ_{corr}, during which a trajectory has not lost memory of its initial conditions. τ_{corr} is short compared to the characteristic diffusion time, τ_{diff}, from the interior of a box to its boundary. In the analysis presented in this paper, τ_{diff} varies from box to box, and we have related τ_{diff} to the slower time scales for box-to-box diffusion. So long as

$$\tau_{\mathrm{diff}} \gg \tau_{\mathrm{corr}} \tag{19}$$

then the "diffusional" picture of box-to-box dynamics is accurate. Inequality 19 may always be met if the boxes are large enough and is the condition of Markovian kinetics when only the transitions between neighboring boxes need to be considered. It is reasonable to assume that eq 19 will hold for large systems with significant anharmonic coupling. The time τ_{kin} for phenomenological kinetics is determined by the eigenvalues of smallest absolute magnitude determined from diagonalization of the matrix **M** and

$$\tau_{\mathrm{kin}} \gg \tau_{\mathrm{diff}} \tag{20}$$

Along with Figure 4, the data in Tables 2 and 3 show that inequality 20 holds. If both conditions, eqs 19 and 20, are met, then the phenomenological kinetics obtained from **M** are largely insensitive to the number of boxes and their size.

7. DISCUSSION AND CONCLUSIONS

In this paper, we have considered in further detail the recently developed boxed molecular dynamics method and shown that a proper accounting for dynamical effects on time scales shorter than that of dynamical decorrelation is important for obtaining accurate kinetics. However, in calculating free energy surfaces, the dynamical effects largely cancel, making BXD a robust method for calculating free energies in the ergodic limit.

We have also discussed the interrelations between BXD and Markovian milestoning (MMS). The manner in which the free energy surfaces are calculated in both BXD and MMS is not sensitive to dynamical decorrelation, which is interesting *per se*, and both methods give similar long time kinetics decay traces. The primary difference between the two methods is in their uncorrected short time behavior, where each is subject to different types of nonstatistical effects: BXD overestimates the decay rate for going from one box to another, while MMS underestimates it. For the system considered in this work, overestimation introduces more error than underestimation, although it is in principle possible to imagine a situation where the MMS lag may lead to overestimation of the box-to-box transition time.

Scheme 4. Extended BXD Scheme That We Will Investigate in Further Work[a]

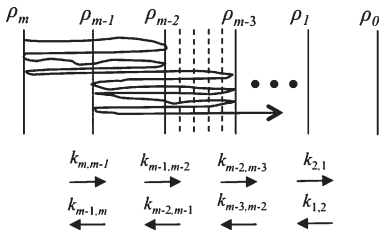

[a] The method is similar to that illustrated in Scheme 2, with the primary difference being the overlap in consecutive box dynamics.

Removing the very fast short-time dynamical effects from BXD provides a set of box-to-box MFPTs that allows an accurate calculation of both the free energy and the kinetics along a particular reaction coordinate. This insight should prove useful to users of BXD following its recent implementation in CHARMM[55] and is inituitively appealing insofar as it is provides a set of mean first passage times which are compatible with the manner in which molecular modellers typically tend to think of a reaction: i.e., transition from a reactant configuration space volume to a product configuration space volume. This enables one to avoid using separate sets of rate coefficients for the free energies and kinetics, distinct from the current MMS protocol. Of further interest is the fact that BXD includes a specification for an exact renormalization procedure,[28] which we have found suffers from few of the numerical problems often associated with the WHAM procedure used to reweight umbrella sampling simulations. The BXD renormalization procedure should also be applicable to MMS.

Another feature of AXD and BXD which we believe to be of practical convenience is that the velocity inversion procedure preserves angular momentum, linear momentum, and energy, making it useful for accelerating both equilibrium and nonequilibrium dynamics. This method for doing velocity inversion has recently enabled application of AXD to nonequilibrium molecular dynamics simulations (NEMD)[56] to accelerate solution phase reaction dynamics. Along the same lines, we note that there may be cases where the initial nonstatistical dynamical behavior, which is preserved by AXD and BXD, is of fundamental interest.

Figure 5 illustrates another point regarding the restricted dynamics used by both BXD and MMS. At times longer than the MMS lag or the BXD τ_{corr}, the logarithmic decay plot is not a perfectly straight line, slowing noticeably at times longer than $\sim 2 \times 10^4$ fs. More generally, this points to the fact that associating the BXD and MMS decays with a single rate constant may be an oversimplification. For this reason, we chose herein to emphasize mean first passage times in the description of BXD. As shown in our previous article, this procedure results in BXD giving free energies that agree well with those obtained in unbiased simulations.[28]

In further work, we plan to extend BXD to multidimensional reaction coordinates; the recent use of Voronoi tessellations in MMS offers a possible way forward.[7,57] Additionally, we plan to investigate an extended version of BXD, which is shown in Scheme 4. In this extension of BXD, $\Delta G_{n-1,n}$ (the free energy difference between two boxes $n-1$ and n) may be determined by constrained dynamics in overlapping boxes. This will allow free passage between consecutive boxes which is unperturbed by inversion. Exploiting ergodicity, the free energy difference between regions in any box may then be written as a ratio of the times spent by the trajectory in each region of the box:

$$\exp\left(\frac{-\Delta G_{n-1,n}}{kT}\right) = \frac{P_n}{P_{n-1}} = \frac{\tau_n}{\tau_{n-1}} \qquad (21)$$

By matching up the probabilities for each of the overlapping boxes, it will be possible to construct a free energy profile to higher resolution along the entire reaction coordinate.

AUTHOR INFORMATION

Corresponding Author
*E-mail: david.r.glowacki@bristol.ac.uk.

ACKNOWLEDGMENT

We thank Eric Vanden-Eijnden, Ron Elber, Maddalena Venturoli, and Benoit Roux for a useful exchange that motivated this study.

REFERENCES

(1) Maragliano, L.; Vanden-Eijnden, E.; Roux, B. Free Energy and Kinetics of Conformational Transitions from Voronoi Tessellated Milestoning with Restraining Potentials. *J. Chem. Theory Comput.* **2009**, *5*, 2589.
(2) Zuckerman, D. M.; Woolf, T. B. Efficient dynamic importance sampling of rare events in one dimension. *Phys. Rev. E* **2001**, *63*, 10.
(3) Henin, J.; Chipot, C. Overcoming free energy barriers using unconstrained molecular dynamics simulations. *J. Chem. Phys.* **2004**, *121*, 2904.
(4) Kinnear, B. S.; Jarrold, M. F.; Hansmann, U. H. E. All-atom generalized-ensemble simulations of small proteins. *J. Mol. Graphics Modell.* **2004**, *22*, 397.
(5) Frenkel, D.; Smit, B. *Understanding Molecular Simulation*, 2nd ed.; Academic Press: London, 2002.
(6) Darve, E.; Rodriguez-Gomez, D.; Pohorille, A. Adaptive biasing force method for scalar and vector free energy calculations. *J. Chem. Phys.* **2008**, *128*, 144120/1.
(7) Vanden-Eijnden, E.; Venturoli, M. Markovian milestoning with Voronoi tessellations. *J. Chem. Phys.* **2009**, *130*, 194101/1.
(8) Vanden-Eijnden, E.; Venturoli, M.; Ciccotti, G.; Elber, R. On the assumptions underlying milestoning. *J. Chem. Phys.* **2008**, *129*, 174102/1.
(9) Kumar, S.; Bouzida, D.; Swendsen, R. H.; Kollman, P. A.; Rosenberg, J. M. The weighted histogram analysis method for free-energy calculations on biomolecules. I. The method. *J. Comput. Chem.* **1992**, *13*, 1011.
(10) Voter, A. F. A method for accelerating the molecular dynamics simulation of infrequent events. *J. Chem. Phys.* **1997**, *106*, 4665.
(11) Voter, A. F. Hyperdynamics: accelerated molecular dynamics of infrequent events. *Phys. Rev. Lett.* . **1997**, *78*, 3908.
(12) Voter, A. F.; Montalenti, F.; Germann, T. C. Extending the time scale in atomistic simulation of materials. *Annu. Rev. Mater. Res.* **2002**, *32*, 321.
(13) Torrie, G. M.; Valleau, J. P. Non-physical sampling distributions in monte-carlo free-energy etsimation - umbrella sampling. *J. Comput. Phys.* **1977**, *23*, 187.
(14) Faradjian, A. K.; Elber, R. Computing time scales from reaction coordinates by milestoning. *J. Chem. Phys.* **2004**, *120*, 10880.
(15) Chipot, C.; Henin, J. Exploring the free-energy landscape of a short peptide using an average force. *J. Chem. Phys.* **2005**, *123*, 244906/1.
(16) Laio, A.; Parrinello, M. Escaping free-energy minima. *Proc. Natl. Acad. Sci. U. S. A.* **2002**, *99*, 12562.

(17) Carter, E. A.; Ciccotti, G.; Hynes, J. T.; Kapral, R. Constrained reaction coordinate dynamics for the simulation of rare events. *Chem. Phys. Lett.* **1989**, *156*, 472.
(18) Huber, T.; Torda, A. E.; van Gunsteren, W. F. Local elevation: a method for improving the searching properties of molecular dynamics simulation. *J. Comput.-Aided Mol. Des.* **1994**, *8*, 695.
(19) Sprik, M.; Ciccotti, G. Free energy from constrained molecular dynamics. *J. Chem. Phys.* **1998**, *109*, 7737.
(20) Paci, E.; Ciccotti, G.; Ferrario, M.; Kapral, R. Activation Energies by Molecular Dynamics with Constraints. *Chem. Phys. Lett.* **1991**, *176*, 581.
(21) Ciccotti, G.; Ferrario, M. Blue moon approach to rare events. *Mol. Simul.* **2004**, *30*, 787.
(22) Grubmuller, H. Predicting Slow Structural Transitions in Macromolecular Systems - Conformational Flooding. *Phys. Rev. E* **1995**, *52*, 2893.
(23) Hummer, G. Fast-growth thermodynamic integration: Error and efficiency analysis. *J. Chem. Phys.* **2001**, *114*, 7330.
(24) Woods, C. J.; Essex, J. W.; King, M. A. The development of replica-exchange-based free-energy methods. *J. Phys. Chem. B* **2003**, *107*, 13703.
(25) Jarzynski, C. Equilibrium free-energy differences from nonequilibrium measurements: A master-equation approach. *Phys. Rev. E* **1997**, *56*, 5018.
(26) Warmflash, A.; Bhimalapuram, P.; Dinner, A. R. Umbrella sampling for nonequilibrium processes. *J. Chem. Phys.* **2007**, *127*, 8.
(27) Vanden-Eijnden, E. Some Recent Techniques for Free Energy Calculations. *J. Comput. Chem.* **2009**, *30*, 1737.
(28) Glowacki, D. R.; Paci, E.; Shalashilin, D. V. Boxed molecular dynamics: a simple and general technique for accelerating rare event kinetics and mapping free energy in large molecular systems. *J. Phys. Chem. B* **2009**, *113*, 16603.
(29) Martinez-Nunez, E.; Shalashilin, D. V. Acceleration of Classical Mechanics by Phase Space Constraints. *J. Chem. Theory Comput.* **2006**, *2*, 912.
(30) Shalashilin, D. V.; Thompson, D. L. Monte Carlo Variational Transition-State Theory Study of the Unimolecular Dissociation of RDX. *J. Phys. Chem. A* **1997**, *101*, 961.
(31) Guo, Y.; Shalashilin, D. V.; Krouse, J. A.; Thompson, D. L. Intramolecular dynamics diffusion theory approach to complex unimolecular reactions. *J. Chem. Phys.* **1999**, *110*, 5521.
(32) Guo, Y.; Shalashilin, D. V.; Krouse, J. A.; Thompson, D. L. Predicting nonstatistical unimolecular reaction rates using Kramers' theory. *J. Chem. Phys.* **1999**, *110*, 5514.
(33) Shalashilin, D. V.; Thompson, D. L. Method for predicting IVR-limited unimolecular reaction rate coefficients. *J. Chem. Phys.* **1997**, *107*, 6204.
(34) Shalashilin, D. V.; Thompson, D. L. Intramolecular dynamics diffusion theory: nonstatistical unimolecular reaction rates. *ACS Symp. Ser.* **1997**, *678*, 81.
(35) Skinner, J. L.; Wolynes, P. G. Relaxation Processes and Chemical Kinetics. *J. Chem. Phys.* **1978**, *69*, 2143.
(36) Chandler, D. Statistical Mechanics of isomerization Dynamics in Liquids and Transition State Approximation. *J. Chem. Phys.* **1978**, *68*, 2959.
(37) Montgomery, J. A.; Chandler, D.; Berne, B. J. Trajectory analysis of a kinetic theory for isomerization dynamics in condensed phases. *J. Chem. Phys.* **1979**, *70*, 4056.
(38) Voter, A. F.; Doll, J. D. Dynamical Corrections to Transition State Theory for Multistate Systems - Surface Self-Diffusion in the Rare-Event Regime. *J. Chem. Phys.* **1985**, *82*, 80.
(39) Elber, R. A milestoning study of the kinetics of an allosteric transition: Atomically detailed simulations of deoxy Scapharca hemoglobin. *Biophys. J.* **2007**, *92*, L85.
(40) Kuczera, K.; Jas, G. S.; Elber, R. Kinetics of Helix Unfolding: Molecular Dynamics Simulations with Milestoning. *J. Phys. Chem. A* **2009**, *113*, 7461.
(41) West, A. M. A.; Elber, R.; Shalloway, D. Extending molecular dynamics time scales with milestoning: example of complex kinetics in a solvated peptide. *J. Chem. Phys.* **2007**, *126*, 145104.
(42) Feige, M. J.; Paci, E. Rate of Loop Formation in Peptides: A Simulation Study. *J. Mol. Biol.* **2008**, *382*, 556.
(43) Paci, E.; Lindorff-Larsen, K.; Dobson, C. M.; Karplus, M.; Vendruscolo, M. Transition State Contact Orders Correlate with Protein Folding Rates. *J. Mol. Biol.* **2005**, *352*, 495.
(44) Ferrara, P.; Apostolakis, J.; Caflisch, A. Evaluation of a fast implicit solvent model for molecular dynamics simulations. *Proteins* **2002**, *46*, 24.
(45) Lourderaj, U.; Hase, W. L. Theoretical and Computational Studies of Non-RRKM Unimolecular Dynamics. *J. Phys. Chem. A* **2009**, *113*, 2236.
(46) There are a number of schemes for removing recrossing. In this particular case, we found that it was easy to remove recrossing for the decays in Figure 1 using fits to a biexponential of the form $R(t) = A\exp(-k_f t) + B\exp(-k_s t)$ where the sum $A + B$ is constrained to give $R(0)$, and k_f and k_s are the respective rate coefficients for the fast and slow components of the $R(t)$ decay.
(47) Buchete, N. V.; Hummer, G. Coarse master equations for peptide folding dynamics. *J. Phys. Chem. B* **2008**, *112*, 6057.
(48) Chodera, J. D.; Singhal, N.; Pande, V. S.; Dill, K. A.; Swope, W. C. Automatic discovery of metastable states for the construction of Markov models of macromolecular conformational dynamics. *J. Chem. Phys.* **2007**, *126*, 155101/1.
(49) Bowman, G. R.; Beauchamp, K. A.; Boxer, G.; Pande, V. S. Progress and challenges in the automated construction of Markov state models for full protein systems. *J. Chem. Phys.* **2009**, *131*, 124101/1.
(50) Glowacki, D. R.; Pilling, M. J. Unimolecular Reactions of Peroxy Radicals in Atmospheric Chemistry and Combustion. *ChemPhysChem* **2010**, *11*, 3836.
(51) Gillespie, D. T. Stochastic simulation of chemical kinetics. *Annu. Rev. Phys. Chem.* **2007**, *58*, 35.
(52) Miller James, A.; Klippenstein Stephen, J. Master equation methods in gas phase chemical kinetics. *J. Phys. Chem. A* **2006**, *110*, 10528.
(53) Wales, D. J. Energy landscapes: calculating pathways and rates. *Int. Rev. Phys. Chem.* **2006**, *25*, 237.
(54) Bartis, J. T.; Widom, B. Stochastic Models of Interconversion of 3 or more Chemical Species. *J. Chem. Phys.* **1974**, *60*, 3474.
(55) Brooks, B. R.; Brooks, C. L., III; Mackerell, A. D., Jr.; Nilsson, L.; Petrella, R. J.; Roux, B.; Won, Y.; Archontis, G.; Bartels, C.; Boresch, S.; Caflisch, A.; Caves, L.; Cui, Q.; Dinner, A. R.; Feig, M.; Fischer, S.; Gao, J.; Hodoscek, M.; Im, W.; Kuczera, K.; Lazaridis, T.; Ma, J.; Ovchinnikov, V.; Paci, E.; Pastor, R. W.; Post, C. B.; Pu, J. Z.; Schaefer, M.; Tidor, B.; Venable, R. M.; Woodcock, H. L.; Wu, X.; Yang, W.; York, D. M.; Karplus, M. CHARMM: The biomolecular simulation program. *J. Comput. Chem.* **2009**, *30*, 1545.
(56) Greaves, S. J.; Rose, R. A.; Oliver, T. A. A.; Glowacki, D. R.; Ashfold, M. N. R.; Harvey, J. N.; Clark, I. P.; Greetham, G. M.; Parker, A. W.; Towrie, M.; Orr-Ewing, A. J. Vibrationally Quantum-State–Specific Reaction Dynamics of H Atom Abstraction by CN Radical in Solution. *Science* **2011**, *331*, 1423.
(57) Vanden-Eijnden, E.; Venturoli, M. Revisiting the finite temperature string method for the calculation of reaction tubes and free energies. *J. Chem. Phys.* **2009**, *130*, 17.